Response of sediment phosphorus partitioning to lanthanum-modified clay amendment and porewater chemistry in a small eutrophic lake.

Wessam Neweshy, Dolors Planas, Elisabeth Tellier, Remi Marsac, Marie Demers, Raoul-Marie Couture

Environmental Science
Processes & Impacts

Accepted Manuscript

This article can be cited before page numbers have been issued, to do this please use: W. Neweshy, D. Planas, E. Tellier, R. Marsac, M. Demers and R. Couture, *Environ. Sci.: Processes Impacts*, 2022, DOI: 10.1039/D1EM00544H.

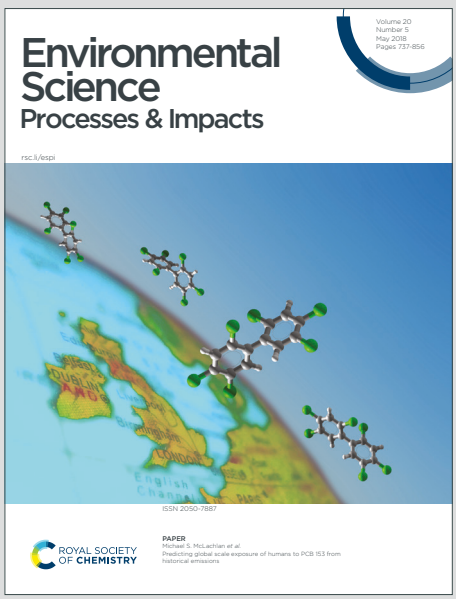

View Article Online
DOI: 10.1039/D1EM00544H

120 WORDS ENVIRONMENTAL SIGNIFICANCE STATEMENT

Eutrophication of lake ecosystems is a pervasive global environmental problem. Excess loading of the nutrient phosphorus from human activities in catchment areas cause lakes to fall into eutrophic states from which natural recovery is slow. As such, measures designed to retain nutrients in sediments, and limit internal nutrient loads, are widely studied. Here, we document the response of sediment solid-phase and porewater geochemistry to a prevalent chemically based phosphorus remediation technique based the addition of lanthanum-modified clay. We use field and modelling evidence to reveal the diagenetic partitioning of phosphorus with lanthanum and Fe (oxy)hydroxides. We suggest that the reported ability of dissolved organic carbon to lower treatment efficacy depends on the absence of ferrous iron.

View Article Online
DOI: 10.1039/D1EM00544H

Response of sediment phosphorus partitioning to lanthanum-modified clay amendment and porewater chemistry in a small eutrophic lake.

Wessam Neweshy[1], Dolors Planas[2], Elisabeth Tellier[3], Marie Demers[1], Remi Marsac[4] and Raoul-Marie Couture[1,*]

1- Department of chemistry, Université Laval, Québec Canada and GRIL (Interuniversity Research Group in Limnology)
2- Département de Sciences Biologiques, Université de Québec à Montréal, Montréal, Canada and GRIL (Interuniversity Research Group in Limnology)
3- Action Conservation du Bassin Versant du Lac Bromont, Bromont, Québec, Canada
4- Univ Rennes, CNRS, Géosciences Rennes - UMR 6118, F-35000 Rennes, France

* Corresponding author: raoul.couture@chm.ulaval.ca

0. Abstract

Sustained eutrophication of the aquatic environment by the remobilization of legacy phosphorus (P) stored in soils and sediments is a prevailing issue worldwide. Fluxes of P from the sediments to the water column, referred to as internal P loading, often delays the recovery of water quality following a reduction in external P loads. Here, we report on the vertical distribution and geochemistry of P, lanthanum (La), iron (Fe) and carbon (C) in the culturally eutrophied Lake Bromont. This lake underwent remediation treatment using La- modified bentonite (LMB) commercially available as Phoslock™. We investigated the effectiveness of LMB in decreasing soluble reactive phosphorus (SRP) availability in sediments and in reducing dissolved fluxes of P across the sediment-water interface. Sediment cores were retrieved before and after LMB treatment at three sites representing bottom sediment, sediment influenced by lakeside housing and finally littoral sediment influenced by the lake inflow. Sequential extractions were used to assess changes in P speciation. Depth profiles of dissolved porewater concentrations were obtained after LMB treatment at each site. Results indicate that SRP extracted from the

View Article Online
DOI: 10.1039/D1EM00544H

sediments decreased at all sites, while total extracted P (P_{TOT}) bound to redox-sensitive metal oxides increased. ^{31}P NMR data on P extract reveals that 20-43% of total solid-phase P is in the form of organic P (P_{org}) susceptible to be released via microbial degradation. Geochemical modelling of porewater data provides evidence that $LaPO_{4(s)}$ mineral phases, such as rhabdophane and/or monazite, are likely forming. However, results also suggest that La^{3+} binding by dissolved organic carbon (DOC) hinders La-phosphate precipitation. We rely on thermodynamic modelling to suggest that high Fe^{2+} would bind to DOC instead of La^{3+}, therefore promoting P sequestrations by LMB under anoxic conditions.

1. Introduction

Harmful freshwater algae blooms negatively impact water quality, which is detrimental to public health and aquatic ecosystems globally[1]. In lake ecosystems, inadequate management of external nutrient loads, namely phosphorus (P) and nitrogen (N), is often the culprit. Decisive actions on improving catchment nutrient loads are, however, not often met with immediate results and legacy nutrients from within the catchment and from within the lake's sediments can be released long after such appropriate actions are taken[2]. It is generally accepted that internal nutrient loads are responsible for the observed decoupling between management actions and water quality responses [3-7]. Even though dual nutrient limitations by both P and N is widespread [8, 9], lakes can be impacted more severely by excess P rather than by excess N [10]. For such lakes, managers are justified to focus their economic and logistical efforts on P reduction to limit excessive algal biomass growth and are often faced with internal P sources that endure after external sources are abated.

View Article Online
DOI: 10.1039/D1EM00544H

In view of the pervasive nature of internal P load, the role of sediments in supplying P and the coupling of the biogeochemical cycling of P with that of other key elements is intensely studied[11]. Internal sediment sources of P can be understood as pools with specific reactivities, susceptible to mobilization as bottom water chemistry fluctuates[10]. Organic P (P_{org}) can be accumulated as biomass or bound to sedimentary organic carbon (C_{org})[12]. P_{org} can be derived externally from vegetation or organic material leached from the watershed (allochthonous) or generated in situ (autochthonous) from algal blooms occurring, in particular during the spring and summer. Finally, inorganic P is scarce in the undisturbed catchment, as it is released from weathering, but abundant in the sediment porewater, when it is regenerated during mineralization of P_{org} [13]. Upon its release to the porewater, inorganic P can be adsorbed to redox-sensitive (e.g. Fe) or pH-sensitive (e.g. Al or Ca) mineral surfaces [14].

A host of approaches have been proposed to artificially inhibit internal nutrient loading, with the aim of lowering nutrient fluxes from sediments to stem cyanobacterial growth and decrease eutrophication. Such approaches can be either physically or chemically based. Physical approaches include dredging and removal of sediment, hypolimnetic withdrawal, and hypolimnetic circulation [15]. Chemical approaches include hypolimnetic oxygenation (along with mixing), flocculation [16-18], and sediment capping [4, 19]. Here, we focus on the outcome of a specific approach to sediment capping that relies on La-modified bentonite (LMB), commercially available as Phoslock™ [20, 21]. With this product, clay is modified by replacing cations within the exchangeable layer that resides between the two tetrahedral-octahedral-tetrahedral structures by a layer of La^{3+}. La^{3+} is released upon LMB addition to the lake's water and captures P to form rhabdophane ($LaPO_4.nH_2O_{(s)}$), which ages into monazite ($LaPO_{4(s)}$) (log

View Article Online
DOI: 10.1039/D1EM00544H

K= 10^{-26}) over time. LMB was introduced to the market by CSIRO [21, 22] and has been used in many lakes worldwide [23].

LMB is often applied using the recommended dose of 100:1 LMB :P or 1:1 La:P which is thought to be sufficient to immobilize soluble reactive P (SRP) [24]. Further studies of LMB applications have suggested that the ratio of 100:1 may not always be sufficient due to the interference from other solutes at the P-binding sites of the LMB [19, 20, 24-30]. Alkalinity [31], pH [25] and DOC [32-35] are identified as key factors that can decrease both LMB P-binding capacity as well as the efficiency of the treatment [36].

DOC is as an important parameter that influences the binding capacity of La within LMB [32-34]. In the context of boreal lakes subjected to increasing DOC fluxes [37, 38], where the concentrations of DOC typically range from 4 to 20 mg L^{-1} [39] with highest concentrations found in the sediment porewater, the role of DOC is particularly crucial. For example, Li et al.[35] found that P uptake via LMB depended on the ratio of DOC to P, with uptake suppressed when the C:P molar ratio exceeded 9. To our knowledge, few field-based studies have accessed the geochemical conditions leading to the suppression of P fluxes from the sediments in the presence of DOC.[40] These studies point to a key interplay between La^{3+} , DOC, and Fe [40-42], which we set out to better understand using field data and thermodynamic modelling.

Few studies have measured the vertical distribution of P, La and associated elements in the sediment following treatment [20, 28, 43, 44], which is key given that LMB relies entirely on sediment remediation of P via fixation by La. Similarly, porewater systematics has seldom been measured at an LMB-remediated site after treatment, despite porewater being sensitive indicators of the

View Article Online
DOI: 10.1039/D1EM00544H

reactions taking place in the porous media. Here, we investigate the sequestration of P in the sediments post LMB applications using both sediment and porewater data. We discuss P speciation in the sediment before and after treatment and use porewater concentrations to calculate the speciation La. Specifically, our objectives are to: i) assess dominant P species in the sediment before and after treatment, ii) document P speciation at three sites under contrasting influences from the catchment and iii) interpret porewater profiles in terms of equilibrium La and P speciation, and iv) quantify the effect that DOC has on prevailing equilibria.

2. Material and method:

2.1. Study site.

Lake Bromont (45°15' N 72° 40' W, Fig. 1) is in the municipality of Bromont in southeastern Québec, Canada. It is part of the hydrographic network of the Yamaska River, which itself flows into St. Lawrence River at lake St. Pierre. Formerly a pond, Lake Bromont was formed following the construction of a dam in the 1950s to provide drinking water for the town of Cowansville. The lake has a surface area of 4.6 km^2 at maximum water level of 7.2m. Its average depth is 4.8 m. It is thermally stratified in the summer and develops seasonal anoxia in the summer (up to 121 days in the warm 2010 summer[45]) and likely under ice as many lakes do [46].

2.2. Sediment and water sampling.

Before treatment, sediment cores were collected by the Phoslock™ Europe GmbH company in July 2014 [47], sliced from 0 to 4 and 4 to 10 cm and frozen until analysis using sequential extractions described below. After treatment, we collected sediment cores of 90 mm diameter and 60 cm length in September 2019 at three stations in Lake Bromont using a UWITEC gravity corer (Fig. 1) hereafter referred to as: Deep site, House site, and Inflow site. Before collecting the samples, we measured water column temperature and dissolved oxygen using an YSI EXO-II

View Article Online
DOI: 10.1039/D1EM00544H

multiparameter probe. Three sediment cores were collected at each station. Core 1 was sectioned following the three-section scheme used by the consultants; here we document the first two layers of 0-4 and 4-10 cm for the purpose of before and after treatment comparison. We performed the analysis of the samples from this core in triplicates. Core 2 was extruded with a 1cm resolution from 0 to 40 cm depth and stored at -20 ^{o}C for solid-phase analyses. Core 3 was subsampled for porewater samples using micro rhizons (Rhizosphere product inc.) with a PES filter of 0.2µm pore size from 2 cm above the sediment-water interface down to 12 cm depth. Porewater subsamples were distributed in vials according to the required analysis: 1) 4 ml was delivered in acid-washed PFA bottles with ultra-pure HNO_3 to measure major and trace dissolved elements; 2) 1.5 ml was delivered in Eppendorf tubes to measure the anions; 3) 4ml was delivered to alkaline-washed amber glass bottle acidified with HCl 2N to measure DOC, 4) 2 ml was delivered in 2 ml amber glass bottles containing Zn-acetate to measure total dissolved sulfides.

Discrete duplicate water samples were collected once a month from May to October from 2017 onward with a Van Dorn bottle at the deepest part of the lake at 0.5 m and 6.3 m for the surface and the bottom sample. P_{TOT} was digested in an autoclave at 150 atm with persulphate solution [48] and determined using the molybdenum blue colorimetric method[49,50] .

2.3. Solid phase analysis.

Frozen sediment was freeze-dried and homogenized in an agate mortar. Solid-phase P was extracted using a P fractionation scheme (sequential extraction; SEQ) based on Hupfer et al. 2009 [51] and modified from Huser et al. 2019 [52] (Table 1). 200 mg of dry sediment was weighed and mixed at a 1:50 soil: solution mass ratio using a bench-top roller for the following extraction steps: i) 2 hrs H_2O-step, associated with loosely bound P, ii) 1 hr bicarbonate/dithionite step

View Article Online
DOI: 10.1039/D1EM00544H

(BD) associated with redox-sensitive P bound to Fe and/or Mn oxides, iii) 16 hrs NaOH-step associated with P bound to Fe and or Al oxides, as well as a fraction of organic P, iv) 16 hrs HCl-step associated with P bound to Ca (apatite). Extractions were carried out in acid-washed 15 ml PP centrifuge tubes and centrifuged at 3000×*g* for 10 minutes after each step. Afterward, each supernatant was pipetted into a syringe equipped with 0.45 µm PES membrane filter cartridge, delivered to an acid-washed 12 ml HDPE centrifuge tube and kept at 4 °C until analysis. Total P, Fe and La concentrations in the extracts were analyzed by triple-quadrupole ICP-MS (ICP-QQQ-MS, Agilent model 8900) while soluble reductive phosphorus (SRP) was determined using a Lachat QuikChem 8500 nutrient analyzer. Finally, total organic carbon (TOC) and nitrogen (TN) concentrations in the sediment were analyzed on homogenized freeze-dried sediment after de-carbonatation using a CHNS elemental analyzer (Thermo-Fisher Flash Smart 2000).

P speciation was further evaluated using ^{31}P NMR on liquid solid-phase extracts. P was extracted from suspended samples based on Cade-Menun 2005 [53]. Briefly, ~3g of homogenized freeze-dried sediment sediments were extracted in 25 ml 0.5M NaOH and 0.1M EDTA for 16 hrs at ambient room temperature on a bench-top roller. The tubes were centrifuged at 3500 × *g* for 30 min and the supernatant filtered using a 0.45 PES filter cartridge. The resulting solution was then freeze-dried at -80°C for 48hrs and the dried extract redissolved in a solution of NaOH and EDTA amended with D_2O, then transferred into an NMR glass tube. Three thousand ^{31}P NMR scans were obtained on an Agilent DD2 500 MHz NMR spectrometer equipped with a 5 mm broadband probe using a 90° pulse, 0.7 s acquisition time and 5 s delay, requiring 12 hours per sample. P compounds and ratios were identified by their chemical shift using inorganic orthophosphoric acid standards. Peak area calculations and spectra processing were completed using Mnova v.14 (Mestrelab Research).

View Article Online
DOI: 10.1039/D1EM00544H

2.4. LMB treatment.

A 5-year study of the nutrient inputs to the lake and the influence of nutrients in supporting the proliferation of harmful algae began in spring 2007, following an intensive cyanobacteria bloom in the summer of 2006. *Planktothrix agardhii* and *Aphanizomenon flosaquae*, the cyanobacteria species causing the major bloom in the lake, were growing in the meta-hypolimnion of the lake, where P was abundant and light was sufficient for their photosynthesis requirements [54, 55]. Despite its shallow depth, this lake forms an intermediate-deep layers as a result if its intense thermal stratification during the summer[54]. The study of the lake's P budget based on mass-balance inflow-outflow model established that around 80% of the concentration in the water column was supported by the P internal loading.

Given historical P inputs to the lake and the pool of reactive P species in the top layer of the sediments, LMB was recommended as a capping agent to control internal P fluxes in lake Bromont. LMB typically contains approximately 5% La by weight [56]. The lake's physico-chemical characteristic, i.e. neutral to slightly alkaline pH of the water column, low DOC (< 4 mg/L) and deep-water anoxic conditions during the ice-free season were deemed suitable for such treatment. In the fall 2017, 173.8 tons of LMB were dispersed in the water column to achieve a targeted La:P ratio of 1:1. The dosage aimed to sequester 1639 kg of potentially releasable P in the surface column. The dosage of LMB was calculated to target two P pools: P in the hypolimnion estimated in July 2014 and the releasable P in the sediment collected before treatment, assumed to comprise water-extractable P and BD- extractable P, and P_{org} from NaOH extracts [47 51].

2.5. Porewater analysis.

The concentration of major dissolved elements (i.e., Fe, Mn, Ca) were measured by inductively coupled plasma optical emission spectroscopy (ICP-OES Thermo-Fisher duo iCAP 7400). Trace

View Article Online
DOI: 10.1039/D1EM00544H

element (P, La) concentrations were determined by ICP-QQQ-MS as above. Anion (PO_4^{3-}, NO_3^-, SO_4^{2-}, Cl^-) concentrations were measured by ion chromatography with UV detection (Thermo Dionex model integration HPLC equipped with AS-11 column). Total dissolved sulfide concentrations were analyzed using UV spectroscopy and the Cline reagent [57] on an Horiba Aqualog EEM spectrofluorometer. Finally, DOC analysis was performed using a TOC analyzer (Vario TOC-Cube, Elementar America).

2.6. Thermodynamic modelling.

Thermodynamic modelling was performed with PHREEQC v. 3[58] , a computer code based on an ion-association aqueous model, designed to perform speciation and saturation-index calculations in water. The thermodynamic database "Minteq.v4.dat" provided with PHREEQC was updated with generally accepted reactions and stability constants at 0 M ionic strength and 25°C for La-inorganic anion complexation relevant to the present work (Table 2and references therein). Further, the humic-ion binding model "Model VII" [59] was implemented directly in PHREEQC to simulate metal ion binding by DOC. The use of humic substances as a surrogate for bulk dissolved organic matter (DOM) has been shown to be reasonable for the simulation of metal binding [60]. It was assumed that DOM: (i) comprised 50% C, (ii) was 50% chemically active and (iii) was composed of humic acids (HA) only. The most recently optimized binding parameters for La and HA were taken from [61]. The PHREEQC-Model VII coupling is described elsewhere [62, 63]. Briefly, Model VII assumes that the complexation of ions by HA occurs through various discrete groups (carboxylic and phenolic groups), which can form either mono-, bi- or tri-dentate binding sites. Because HA are large and negatively charged polyelectrolytes or colloids, electrostatic effects are also accounted for the quantification of metal ions-HA binding [59]. Cation competition was considered by including Mn^{2+}, Ca^{2+}, Al^{3+}, Fe^{2+} and Fe^{3+} binding to HA.

View Article Online
DOI: 10.1039/D1EM00544H

Measured aqueous concentrations and bottom water pH (pH = 6.43) were applied to the model to mimic in-situ conditions. The potential precipitation of several minerals was allowed (e.g., pyrite, magnetite, vivianite and $MnHPO_{4(s)}$) in the model. Saturation indices (SI) for the porewater with respect to $LaPO_{4(s)}$ phases were also calculated as a function of depth at the three different sampling sites, using the determined composition of the porewater (inorganic P, Fe, Mn, La, Ca, Na and S, with Cl added for electroneutrality). Finally, the combined effects of $[Fe^{2+}]$ and [DOC] on the percentage of La precipitated as $LaPO_{4(s)}$ was investigated using the software Phreeplot [64], which can draw contour plots from PHREEQC calculations. The porewater composition used for the latter calculations was set to the mean concentrations of all samples analyzed in the present study ([P] = 22.85 µM, [Mn] = 54.50 µM, [Ca] = 507.62 µM, [S] = 24.97 µM, [La] = 29.6 nM). Here, we assumed that the redox potential was controlled by the redox couples O_2/H_2O in the oxygenated overlying waters of the Inflow site, and $Fe(II)/Fe(OH)_{3(s)}$ in porewater samples with HS^- concentrations <1 µM. In all sulfidic samples, hereafter defined as those with HS^- concentrations greater than 1 µM, the redox potential was fixed by the redox couples SO_4^{2-}/HS^- [65].

2.7. Flux calculations across the sediment-water interface.

Inverse diagenetic modelling was used to objectively constrain fluxes of solutes across the sediment-water interface [65, 66]. Porewater profiles were modelled assuming the absence of significant advective flux and at steady state (i.e., $\delta C/\delta t = 0$). The one-dimensional mass conservation equation provided by Boudreau 1997 [67] at steady state was solved using the computer code PROFILE [68] using sediment porosity and the elements' diffusion coefficients as

View Article Online
DOI: 10.1039/D1EM00544H

inputs, to yield fluxes of La, P, and Fe across the sediment-water interface (SWI) at the three sampling sites.

3. Results.

3.1. Vertical distribution of P, Fe, La and C in the sediment.

The comparison of P partitioning was done on the basis of SEQ results performed before and after the LMB treatment using identical protocols at three sampling sites. Here, we present results for the sediment depths at 0-4 cm (Fig. 2) and 4-10 cm (Fig. S2), within which the excess solid-phase La is contained (Fig. 3b,f,j). P_{TOT} extractable by BD and HCl more than doubled after treatment in surface sediment (0-4 cm). Meanwhile P_{TOT} extracted by NaOH decreased by 11-21% depending on the site, with largest decrease observed at the Deep site and the smallest at the Inflow. SRP measurements in the extract follows similar patterns, but with smaller magnitudes, suggesting that P accumulated in the sediment after the treatment is not in the form of SRP. In contrast with the 0-4 cm depth layer, where SEQ before and after treatment lead to clear contrasts, SEQ results were closer together for the 4-10 cm depths layer (Fig. S2). Nevertheless, P_{TOT} extractable by BD and HCl increased slightly at the Deep and Inflow sites, and HCl-P doubled at the House site. As for the 0-4 cm layer, SRP measurements show similar patterns than P_{TOT}.

P concentrations were measured at a 1-cm vertical resolution in the sediment after the LMB treatment. P_{TOT} in the BD, NaOH and HCl fractions are displayed in Fig. 3(a,e,i). The profiles do not show pronounced subsurface peaks. $P_{TOT,}$ mostly comprising of SRP, is highest at the Deep site, followed by the House and Inflow sites. At the Deep site, it reaches a maximum of 79 mmol kg^{-1} at 11cm depth, of 69 mmol kg^{-1} at 5cm and 37.5 mmol kg^{-1} at 7cm at the House and Inflow sites, respectively. P_{TOT} associated with the NaOH fractions dominates P speciation at the Deep

View Article Online
DOI: 10.1039/D1EM00544H

and House sites, while that associated with the HCl step dominates at the Inflow site. HCl-extracted P does not dominate at the House site but demonstrates a sharp peak at the 4-6 cm depth interval.

La and Fe concentrations were analyzed in the same fractions (Fig. 3). Maximum values are found in the HCl fraction, in contrast to P which was highest in the NaOH fraction at both the Deep site and House sites. Sharp peaks of solid-phase HCl- extractable La are found at 3 and 5 cm depth at the Deep and House side, respectively, and to a lesser extent at the Inflow site. La concentrations were below the detection limit (2 $\mu g\ kg^{-1}$) at all depths below 8 cm at the three sites. Finally, P was correlated with La in the HCl-extracts at the Deep ($R^2 = 0.86$) and House ($R^2 = 0.93$) sites, but not at the Inflow site ($R^2 = 0.005$).

TOC and C:N ratios, measured in decarbonated sediments, indicate values centred around 5% C_{org} and a C:N ratio of 10 at the Deep site. While surface values are similar at the House site, a strong increase in TOC is observed below 15 cm depth, reaching 12% at depth and a C:N ratio of 15. Values at the Inflow site are the most variable, with peaks reaching 14% at 9 cm depth and 19% at 13 cm depth along with a minimum at 2% at 15 cm depth. The C:N ratio fluctuations parallel those of TOC.

Finally, ^{31}P NMR indicates the presence of several organic P forms[69] in addition to the dominant inorganic orthophosphate form. Orthophosphate monoesters, diesters, and pyrophosphates (Fig. 4), collectively referred to as P_{org}, represent 15.7%, 43%, and 27% of the P_{TOT} at the Deep, House and Inflow sites respectively (Fig. 4). The P_{org} pool comprises between 70 and 85% of orthophosphates monoesters. As a general trend, P_{org} content decreases with depth at all sites.

View Article Online
DOI: 10.1039/D1EM00544H

3.4. Vertical distribution of dissolved P, La, Fe and C.

The deep site was below the thermocline at the time of sampling (water temperature = 10.8°C), while the two other sites were above the thermocline (19°C). As for oxygen concentrations, the deep site hypolimnion was anoxic (DO <0.1mg/L), while the two other sites were oxygenated during sampling (DO of 7.4 and 6.2 mg/L at the Inflow and House sites, respectively.).

The minimum concentration of porewater PO_4^{3-} is located just above the SWI, ranging between 1 and 1.5 µM at all sites (Fig. 5 a,f,k). The PO_4^{3-} concentration then sharply increases to just below the SWI, where it either remains at peak value at the Deep and Inflow sites, or continually increases with depth at the House site. The highest PO_4^{3-} concentrations in porewater are 39 µM at 12 cm, 45 µM at 12 cm, and 23 µM at 6 cm for the Deep, House, and Inflow sites, respectively (Fig. 5 a,f,k). The measured dissolved Fe profiles parallel those of P with a minimum concentration above the SWI and increases below it. Dissolved Fe reaches 500 µM at the Deep site, two orders of magnitude higher than at the other two sites where it remains between 5-10 µM. Maximum Fe concentrations are around 1219 µM at 4 cm, 813 µM 12 cm, and 322 µM at 12 cm for the Deep, House, and Inflow sites, respectively (Fig. 5 b,g,i). Dissolved La concentrations, assumed to comprise truly dissolved and colloidal fractions passing through the 0.2 mm membrane, were below the detection limit of 0.004 µM above the SWI at the three sites (Fig. 5 c,h,m), increased sharply at or below the SWI and remained at 0.06-0.07 µM between 2-6 cm depth, then decreased further.

SO_4^{2-} shows maximum concentrations above the SWI, around 11 µM at the Deep site and about an order of magnitude higher (80-85 µM) at the other two sites (Fig. 5 d,i,n). SO_4^{2-} sharply decreases below the SWI, at the Deep and House sites, while it decreases linearly at the Inflow site. ΣS^{-II} were below the detection limit of 0.7 µM at the Deep site, while it increased markedly,

View Article Online
DOI: 10.1039/D1EM00544H

along with the decrease in SO_4^{2-}, below the SWI at the House site to reach 10 µM and 5 µM at the Inflow site (Fig. 5). Finally, DOC concentrations were 325 µM at 7 cm, 432 µM at 1 cm, and 422 cm at the SWI, and minimum concentrations were 59 µM at SWI, 84 µM at 11 cm, and 94 µM at 4 cm for the Deep, House, and Inflow sites, respectively (Fig. 5 e,j,o).

3.5. Water-column total P, fluxes at the SWI and saturation indices.

Water-column P_{TOT} remained between 14 and 25 µg/L in the epilimnion of the lake (Fig. S1), and between 21 and 60 µg/L in the hypolimnion, with the notable exception of the months of June, July and August 2017, that is, before the treatment, where it ranged between 96 and 180 µg/L. Post treatment hypolimnetic P_{TOT} concentrations never exceeded 60 µg/L. Fluxes of solutes across the SWI were calculated after curve fitting of the measured profiles using the code PROFILE. At the Deep and Inflow sites, the sediment acts as a source of solutes to the water column. Conversely, it acts as a sink for P at the House site. Calculated P fluxes are seven orders of magnitude higher than La fluxes at all sites, and fivefold lower than Fe fluxes. Maximum values for diffusive fluxes are found at the Deep sites for all species, as shown on Table 3. Finally, P fluxes before treatment were taken from Planas & Juneau (2019)[70].

Thermodynamic modelling (Fig. 6) of La speciation based on porewater chemistry (Fig. 5, S3 and S4) in the sediments suggests that the porewater are oversaturated with respect to $LaPO_{4(s)}$ minerals below the SWI. However, when accounting for $La^{3+}_{(aq)}$ binding by DOC, the model predicts that the porewater becomes undersaturated with respect to $LaPO_{4(s)}$ at the House and Inflow sites, while they just reach saturation at the Deep site ($-0.05 < SI > 0.05$).

4. Discussion

View Article Online
DOI: 10.1039/D1EM00544H

4.1. Changes in P composition following LMB application.

Monitoring at the sites indicates that both water-column P_{TOT} and cyanobacterial biomass responded to the LMB application[70], consistent with the outcome of other similar treatment and experiments [19, 71-77]. Here, SEQ on vertical sections of sediment cores performed before and after treatment showed a transfer from redox and pH-sensitive P to the more recalcitrant HCl-extractable fraction (Fig. 2), likely consisting of $LaPO_{4(s)}$ [19, 20, 24, 28, 40, 78] as suggested by the correlation between La and P at the Deep and the House sites. The low R^2 at the Inflow might be attributed to very low LMB dose in this site compared to other sites. Nevertheless, the redox-sensitive Fe-bound P increased after applying LMB, in particular at the Deep site, possibly linked to the bentonite being a source of Fe as well as of La. This suggests a partitioning of P within the LMB layer involving not only La but also redox-sensitive Fe oxyhydroxides, consistent with the close coupling between porewater P and Fe (Fig. 5). Reductive dissolution of Fe oxyhydroxides and the concomitant release of redox-sensitive P is also consistent with the observation made that anoxia could release P from LMB.[33]

SEQ with 1-cm vertical resolution (Fig. 3) showed that the Deep and House sites contain an important fraction of pH-sensitive P and organic-P [51], data supported by results from ^{31}P NMR (Fig. 4). Via a transfer from di- to mono-ester in the sediment [79, 80], P_{org} is immobilized by LMB [81] when given enough time, although the stability of this association remains poorly constrained given that P_{org} is labile towards microbial degradation. Nevertheless, sharp solid-phase P peaks that parallel those of La (Fig. 3b,f,j) at the House site suggest a coupling in line with the formation of $LaPO_{4(s)}$ species [19, 20, 24, 28, 78].

The remobilisation of La along with redox-sensitive Fe (Fig. 5) suggests an interplay with Fe oxyhydroxides, likely via the adsorption of the La^{3+} cation. An enhanced mobility of La^{3+} ions

View Article Online
DOI: 10.1039/D1EM00544H

promoted by DOC complexation might explain this association with Fe. Such redox dynamics are absent from the littoral Inflow site. At this site, the sediment contains one tenth of the sedimentary La and Fe found at the other two sites, potentially indicating the presence of acid-soluble organics or carbonates in addition to La-bound P. The low La content is consistent with sediment accumulation from the material introduced by stream water and with smaller proportion of LMB settling at this littoral site after LMB application.

4.3. Coupling of P cycling to that of Fe, La and DOC.

At or below the SWI of all sites, dissolved P, Fe and La concentrations increase along sharp gradients (Fig. 5b, g, l), consistent with removal of aqueous species from the porewater. Thermodynamic calculations, accounting for the effect of DOC in complexing La^{3+}, show that the porewater are oversaturated with respect to $LaPO_{4(s)}$ at the SWI of all sites. Oversaturation suggests that the solid $LaPO_{4(s)}$ may precipitate, but is either kinetically hindered, as has a been observed previously for stable minerals such as pyrite [82] or that La colloids have passed through the 0.2 mm filter membranes, leading to an over estimation of dissolved La [31] At the House and Inflow sites, which both display higher porewater DOC concentration at the SWI, accounting for DOC in the thermodynamic calculation shifts the SI by several orders of magnitude away from saturation with respect to $LaPO_{4(s)}$ (Fig. 6), although this is limited to a zone just below the SWI. This is in line with previous studies that have suggested the competition between PO_4^{3-} and other anions for complexation with $La^{3+}_{(aq)}$, given that La-DOC is a thermodynamically favourable complex [61].

While our conclusion holds for the date of sampling given the model inputs, notably the measured dissolved Fe concentrations, it thus depends on variations in Fe^{2+} caused by seasonal bottom water dissolved oxygen depletion. With the caveat that we did not ascertain vivianite

View Article Online
DOI: 10.1039/D1EM00544H

formation [83, 84], our calculation suggests that $Fe^{2+}_{(aq)}$ binds strongly to DOC as it is present, in Lake Bromont porewater, at concentrations 2 to 3-fold higher than DOC. $Fe^{2+}_{(aq)}$ could thus effectively negate DOC's effect on La^{3+} by freeing the latter to bind to PO_4^{3-} and form $LaPO_{4(s)}$.

The prevalence of Fe^{2+} strongly depends on redox conditions. Under oxygenated conditions, Fe^{2+} is rapidly oxidized to Fe^{3+} and precipitates as Fe oxyhydroxides [85]. In an oxic system dominated by Fe oxyhydroxides, DOC is available to bind La^{3+}, with available PO_4^{3-} adsorbing on the freshly precipitated Fe^{3+} oxyhydroxides [24, 33, 34, 61]. Visual inspection of the profiles on Fig. 5 suggests that the release of porewater P is closely coupled to that of Fe rather than La below the depth of $LaPO_{4(s)}$ formation. Such coupling typically responds to seasonal oxygen depletion, which results in the recycling of PO_3^{4-} along with that of Fe (oxy)hydroxides, a chief cause of internal P loading [4-7, 86, 87]. Under such scenario where Fe fluxes exceed those of P across the SWI, well oxygenated bottom waters are desirable to maintain low P fluxes from the sediment to the bottom water [88].

Dissolved Fe concentrations at depth in the porewater are tightly coupled to those of sulfides. Evidence of SO_4^{2-} reduction (Fig. 5d,i,n) indicate that Fe titrate sulfides out of the porewater at the Deep site. ΣS^{-II} accumulate in the porewater at the House site and to a lesser extent at the Inflow site. Residual HS^- may promote the reductive dissolution of Fe oxides, further releasing P adsorbed onto the oxide's surfaces [89, 90]. While porewater P was stable with depth after its initial increase at the Deep and Inflow sites, it increased continuously at the House site (Fig. 5f). A layer of buried P_{org} (Fig 3e) would be responsible for this supply to the porewater, testifying to historical inputs from septic tank overflow from the lakeside properties.

In a recent series of incubation experiments testing the effect of light and benthic photosynthesis on LMB efficacy, Li et al [91] found that the latter was lowered by photosynthesis, and ascribed it

View Article Online
DOI: 10.1039/D1EM00544H

an increase in pH and to the release of DOC in the form of exudates from the algae. Through their reported concurrent increase in DO was not discussed as a factor in the reduction in LMB efficacy, we find it consistent with DO allowing DOC to freely bind La^{3+} by lowering dissolved Fe^{2+}. Thus, contrary to the intuition that oxic conditions prevent PO_4^{3-} mobility, LMB treated lakes could sequester P more effectively under anoxic and ferruginous conditions. This hypothesis is in line with the outcome of oxic vs anoxic laboratory experiments LMB, which shows that it decreased P fluxes from the SWI under anoxic conditions, but not under oxic conditions [92]. Hence, we have generalized this hypothesis and used the thermodynamic model to illustrate (Fig. 7) that Fe^{2+} and DOC are antagonistic with respect to their influence on $LaPO_{4(s)}$ formation. However, our interpretation does not account for kinetic aspects of the effect of DOC on LMB capacity, which remains unclear.

DOC can also hinder La^{3+} uptake by LMB via the competitive sorption DOC as shown by Li et al. [35]. These authors reported that DOC didn't influence the absorption of P when the C:P molar ratio was ~1.5 or higher. However, the influence of DOC was significant when the molar ratio exceeded 9. As for Lake Bromont, the C:P ratio exceeds this reported threshold, suggesting that DOC not only binds La^{3+} directly in solution but also likely passivates the LMB. Dithmer et al. [33], in a long-term laboratory study, showed that the adverse effects of DOC on P updake by LMB is not permanent, as DOC can be degraded despite being bound to LMB, and that its complexation of La^{3+} is fully reversible [35]. As such, it is unclear which mechanism – passivation of LMB or complexation of La^{3+} – best accounts for the role of DOC. In both cases, however, the reductive dissolution of Fe oxyhydroxides and the production of porewater Fe^{2+} would be a desirable outcome, shifting the equilibrium away from the LMB-DOC and DOC-La^{3+} complexes.

View Article Online
DOI: 10.1039/D1EM00544H

Sources of uncertainty not accounted for here include further competition by cations such as Ca^{2+}, which can be introduced to the lake via the use of $CaCl_2$ as a de-icing salt. On one hand, Ca^{2+} has been shown to enable PO_4^{3-} binding to humics [93, 94], specifically via ternary complexes [95], which increases P mobility. On the other hand, the adsorption of Ca^{2+} on oxides can increase surface potential, hence favouring PO_4^{3-} adsorption through electrostatic effect [96]. Similarly, changing alkalinity was not accounted for, even though HCO_3^- can compete with PO_4^{3-} for binding with La^{3+} [97, 98] . Alkalinity has also been shown to negatively impact dissolved La, due to low dispersion of LMB aggregates[31]and to it further reducing the efficacy of PO_4^{3-} removal in the presence of DOC[42]. Together, these effects are detrimental to LMB's long-term efficacy.

5. Conclusions.

An application of 174 ton of La-modified bentonite to the eutrophic Lake Bromont (Canada) resulted in an abatement of harmful algae blooms. We show that this treatment induced a shift in P partitioning from the sediment to more recalcitrant phases, away from pH-sensitive and organic P. However, porewater systematics revealed that P remained mobile, in close association with the redox-sensitive Fe cycle. Thermodynamic modelling suggested that DOC plays a key role in mediating this interplay, as it binds La^{3+}, lowering the saturation of the porewater with respect to the key mineral phase, $LaPO_{4(s)}$, which the treatment seeks to promote. Our results show that Fe^{2+} indirectly promotes the formation of $LaPO_{3(s)}$ suggesting that anoxic conditions may improve the longevity of the LMB treatment in the presence of DOC.

Acknowledgements:

We acknowledge Pierre Audet for help with NMR, Serge Groleau for help with ICP-QQQ-MS, Marie-Pierre Varin, Anne-Sophie T. Carrier and Michelle Champagne from ACBVLB for help

View Article Online
DOI: 10.1039/D1EM00544H

during sampling and Sarah-Michelle Cormier for help in the laboratory. We acknowledge funding from the Town of Bromont, and Quebec's Ministère de l'Économie et de l'Innovation. RMC acknowledges funding from the Sentinel North program of Université Laval and from the Global Water Futures project FORMBLOOM (made possible in part thanks to funding from the Canada First Research Excellence Funds), as well as from the National Science and Natural Sciences and Engineering Research Council of Canada thought the Discovery Grant program.

View Article Online
DOI: 10.1039/D1EM00544H

6. References

1. D. R. De Figueiredo, U. M. Azeiteiro, S. M. Esteves, F. J. M. Gonçalves and M. J. Pereira, Microcystin-producing blooms—a serious global public health issue, *Ecotoxicology and Environmental Safety*, 2004, **59**, 151-163.
2. D. M. Orihel, D. W. Schindler, N. C. Ballard, M. D. Graham, D. W. O'Connell, L. R. Wilson and R. D. Vinebrooke, The "nutrient pump:" iron-poor sediments fuel low nitrogen-to-phosphorus ratios and cyanobacterial blooms in polymictic lakes, *Limnology and Oceanography*, 2015, **60**, 856-871.
3. M. Søndergaard, J. P. Jensen and E. Jeppesen, Internal phosphorus loading in shallow Danish lakes, *Hydrobiologia*, 1999, **408**, 145-152.
4. E. B. Welch and G. D. Cooke, Internal phosphorus loading in shallow lakes: importance and control, *Lake and Reservoir Management*, 2005, **21**, 209-217.
5. D. W. Schindler, R. E. Hecky, D. L. Findlay, M. P. Stainton, B. R. Parker, M. J. Paterson, K. G. Beaty, M. Lyng and S. E. M. Kasian, Eutrophication of lakes cannot be controlled by reducing nitrogen input: Results of a 37-year whole-ecosystem experiment, *Proceedings of the National Academy of Sciences*, 2008, **105**, 11254.
6. S. B. Watson, C. Miller, G. Arhonditsis, G. L. Boyer, W. Carmichael, M. N. Charlton, R. Confesor, D. C. Depew, T. O. Höök, S. A. Ludsin, G. Matisoff, S. P. McElmurry, M. W. Murray, R. Peter Richards, Y. R. Rao, M. M. Steffen and S. W. Wilhelm, The re-eutrophication of Lake Erie: Harmful algal blooms and hypoxia, *Harmful Algae*, 2016, **56**, 44-66.
7. M. C. Randall, G. T. Carling, D. B. Dastrup, T. Miller, S. T. Nelson, K. A. Rey, N. C. Hansen, B. R. Bickmore and Z. T. Aanderud, Sediment potentially controls in-lake phosphorus cycling and harmful cyanobacteria in shallow, eutrophic Utah Lake, *Plos One*, 2019, **14**.
8. H. W. Paerl, Controlling eutrophication along the freshwater–marine continuum: Dual nutrient (N and P) reductions are essential, *Estuaries and Coasts*, 2009, **32**, 593-601.
9. H. W. Paerl, J. T. Scott, M. J. McCarthy, S. E. Newell, W. S. Gardner, K. E. Havens, D. K. Hoffman, S. W. Wilhelm and W. A. Wurtsbaugh, It takes two to tango: when and where dual nutrient (N & P) reductions are needed to protect lakes and downstream ecosystems, *Environmental Science & Technology*, 2016, **50**, 10805-10813.
10. D. M. Orihel, D. W. Schindler, N. C. Ballard, M. D. Graham, D. W. O'Connell, L. R. Wilson and R. D. Vinebrooke, The "nutrient pump:" Iron-poor sediments fuel low nitrogen-to-phosphorus ratios and cyanobacterial blooms in polymictic lakes, *Limnology and Oceanography*, 2015, DOI: 10.1002/lno.10076, n/a-n/a.
11. A. D. Steinman and B. M. Spears, *Internal Phosphorus Loading in Lakes*, J. Ross Publishing, Plantation, Florida, USA, 2020.
12. T. I. McLaren, R. J. Smernik, M. J. McLaughlin, T. M. McBeath, J. K. Kirby, R. J. Simpson, C. N. Guppy, A. L. Doolette and A. E. Richardson, Complex Forms of Soil Organic Phosphorus–A Major Component of Soil Phosphorus, *Environmental Science & Technology*, 2015, DOI: 10.1021/acs.est.5b02948.
13. C. Hensen, M. Zabel and H. N. Schulz, in *Marine Geochemistry*, eds. H. D. Schulz and M. Zabel, Springer Berlin Heidelberg, Berlin, Heidelberg, 2006, DOI: 10.1007/3-540-32144-6_6, pp. 207-240.

View Article Online
DOI: 10.1039/D1EM00544H

14. K. R. Reddy, S. Newman, T. Z. Osborne, J. R. White and H. C. Fitz, Phosphorous cycling in the greater everglades ecosystem: legacy phosphorous implications for management and restoration, *Critical Reviews in Environmental Science and Technology*, 2011, **41**, 149-186.
15. T. Jilbert, R.-M. Couture, B. J. Huser and K. Salonen, Preface: Restoration of eutrophic lakes: current practices and future challenges, *Hydrobiologia*, 2020, **847**, 4343-4357.
16. J. N. Connor and G. N. Smith, An effiecient method of appling aluminum salts for sediment phosphorus in activation in lakes, *JAWRA Journal of the American Water Resources Association*, 1986, **22**, 661-664.
17. A. Kuster, A. Kuster and B. Huser, A comparison of aluminum dosing methods for reducing sediment phosphorus release in lakes, *Journal of Environmental Management*, 2020, **261**, 110195.
18. B. J. Huser, S. Egemose, H. Harper, M. Hupfer, H. Jensen, K. M. Pilgrim, K. Reitzel, E. Rydin and M. Futter, Longevity and effectiveness of aluminum addition to reduce sediment phosphorus release and restore lake water quality, *Water Res.*, 2016, **97**, 122-132.
19. B. M. Spears, M. Lürling, S. Yasseri, A. T. Castro-Castellon, M. Gibbs, S. Meis, C. McDonald, J. McIntosh, D. Sleep and F. Van Oosterhout, Lake responses following lanthanum-modified bentonite clay (Phoslock®) application: An analysis of water column lanthanum data from 16 case study lakes, *Water Res.*, 2013, **47**, 5930-5942.
20. S. Meis, B. M. Spears, S. C. Maberly, M. B. O'Malley and R. G. Perkins, Sediment amendment with Phoslock® in Clatto Reservoir (Dundee, UK): Investigating changes in sediment elemental composition and phosphorus fractionation, *Journal of Environmental Management*, 2012, **93**, 185-193.
21. G. B. Douglas and J. A. Adeney, presented in part at the International Association Water Quality Conference on Diffuse Pollution, 1999.
22. M. Robb, B. Greenop, Z. Goss, G. Douglas and J. Adeney, Application of Phoslock an innovative phosphorus binding clay, to two Western Australian waterways: preliminary findings, *Hydrobiologia*, 2003, **494**, 237-243.
23. C. W. Hickey and M. M. Gibbs, Lake sediment phosphorus release management—Decision support and risk assessment framework, *New Zealand Journal of Marine and Freshwater Research*, 2009, **43**, 819-856.
24. K. Reitzel, F. Andersen, S. Egemose and H. Jensen, Phosphate adsorption by lanthanum modified bentonite clay in fresh and brackish water, *Water Res.*, 2013, **47**, 2787-2796.
25. G. Ross, F. Haghseresht and T. Cloete, The effect of pH and anoxia on the performance of Phoslock®, a phosphorus binding clay, *Harmful Algae*, 2008, **7**, 545-550.
26. M. Zamparas, A. Gianni, P. Stathi, Y. Deligiannakis and I. Zacharias, Removal of phosphate from natural waters using innovative modified bentonites, *Applied Clay Science*, 2012, **62-63**, 101-106.
27. H. Márquez-Pacheco, A. M. Hansen and A. Falcón-Rojas, Phosphorous control in a eutrophied reservoir, *Environmental Science and Pollution Research*, 2013, **20**, 8446-8456.
28. S. Meis, B. M. Spears, S. C. Maberly and R. G. Perkins, Assessing the mode of action of Phoslock® in the control of phosphorus release from the bed sediments in a shallow lake (Loch Flemington, UK), *Water Res.*, 2013, **47**, 4460-4473.

View Article Online
DOI: 10.1039/D1EM00544H

29. M. Lürling and F. Van Oosterhout, Case study on the efficacy of a lanthanum-enriched clay (Phoslock®) in controlling eutrophication in Lake Het Groene Eiland (The Netherlands), *Hydrobiologia*, 2013, **710**, 253-263.
30. F. van Oosterhout, E. Goitom, I. Roessink and M. Lürling, Lanthanum from a modified clay used in eutrophication control is bioavailable to the marbled crayfish (Procambarus fallax f. virginalis), *PLOS ONE*, 2014, **9**, e102410.
31. K. Reitzel, K. Balslev and H. S. Jensen, The influence of lake water alkalinity and humic substances on particle dispersion and lanthanum desorption from a lanthanum modified bentonite, *Water Res.*, 2017, **125**, 191-200.
32. B. M. Spears, E. B. Mackay, S. Yasseri, I. D. M. Gunn, K. E. Waters, C. Andrews, S. Cole, M. De Ville, A. Kelly, S. Meis, A. L. Moore, G. K. Nürnberg, F. van Oosterhout, J.-A. Pitt, G. Madgwick, H. J. Woods and M. Lürling, A meta-analysis of water quality and aquatic macrophyte responses in 18 lakes treated with lanthanum modified bentonite (Phoslock®), *Water Res.*, 2016, **97**, 111-121.
33. L. Dithmer, U. G. Nielsen, D. Lundberg and K. Reitzel, Influence of dissolved organic carbon on the efficiency of P sequestration by a lanthanum modified clay, *Water Res.*, 2016, **97**, 39-46.
34. M. Lürling, G. Waajen and F. van Oosterhout, Humic substances interfere with phosphate removal by lanthanum modified clay in controlling eutrophication, *Water Res.*, 2014, **54**, 78-88.
35. X. Li, J. Chen, Z. Zhang, Y. Kuang, R. Yang and D. Wu, Interactions of phosphate and dissolved organic carbon with lanthanum modified bentonite: Implications for the inactivation of phosphorus in lakes, *Water Res.*, 2020, **181**, 115941.
36. M. Lürling and M. Mucci, Mitigating eutrophication nuisance: in-lake measures are becoming inevitable in eutrophic waters in the Netherlands, *Hydrobiologia*, 2020, **847**, 4447-4467.
37. G. Algesten, S. Sobek, A.-K. Bergström, A. Ågren, L. J. Tranvik and M. Jansson, Role of lakes for organic carbon cycling in the boreal zone, *Global Change Biology*, 2004, **10**, 141-147.
38. A. G. Finstad, T. Andersen, S. Larsen, K. Tominaga, S. Blumentrath, H. A. de Wit, H. Tømmervik and D. O. Hessen, From greening to browning: Catchment vegetation development and reduced S-deposition promote organic carbon load on decadal time scales in Nordic lakes, *Scientific Reports*, 2016, **6**, 31944.
39. S. Sobek, L. J. Tranvik, Y. T. Prairie, P. Kortelainen and J. J. Cole, Patterns and regulation of dissolved organic carbon: An analysis of 7,500 widely distributed lakes, *Limnology and Oceanography*, 2007, **52**, 1208-1219.
40. L. Dithmer, U. G. Nielsen, M. Lürling, B. M. Spears, S. Yasseri, D. Lundberg, A. Moore, N. D. Jensen and K. Reitzel, Responses in sediment phosphorus and lanthanum concentrations and composition across 10 lakes following applications of lanthanum modified bentonite, *Water Res.*, 2016, **97**, 101-110.
41. M. L. Waajen, B. Engels and F. V. Oosterhout, Effects of Dredging and Lanthanum-Modified Clay on Water Quality Variables in an Enclosure Study in a Hypertrophic Pond, *Water*, 2017, **9**.
42. Y. Zhi, D. F. Call, K. D. Grieger, O. W. Duckworth, J. L. Jones and D. R. U. Knappe, Influence of natural organic matter and pH on phosphate removal by and filterable lanthanum release from lanthanum-modified bentonite, *Water Res.*, 2021, **202**, 117399.

View Article Online
DOI: 10.1039/D1EM00544H

43. S. Yasseri and T. S. Epe, Analysis of the La:P ratio in lake sediments – Vertical and spatial distribution assessed by a multiple-core survey, *Water Res.*, 2016, **97**, 96-100.
44. F. van Oosterhout, G. Waajen, S. Yasseri, M. Manzi Marinho, N. Pessoa Noyma, M. Mucci, G. Douglas and M. Lürling, Lanthanum in Water, Sediment, Macrophytes and chironomid larvae following application of Lanthanum modified bentonite to lake Rauwbraken (The Netherlands), *Science of The Total Environment*, 2020, **706**, 135188.
45. D. Planas and C. Vanier, *Le programme de recherche sur les cyanobactéries: synthèse, conclusions et recommandation*, Service aux collectivités, UQAM, Montréal (Québec), 2014.
46. X. Fang and H. Stefan, Simulated climate change effects on dissolved oxygen characteristics in ice-covered lakes, *Ecological Modelling* 1997, **103**, 209-229.
47. P. Van Goethem, S. Yasseri and N. Traill, *Sediment P-fractionation Lac Bromont - Final report*, Phoslock Europe GmbH, 2014.
48. D. W. Menzel and N. Corwin, The measurement of total phosphorus in seawater based on the liberation of organically bound fractions by persulfate oxidation, *Limnology and Oceanography*, 1965, **10**, 280-282.
49. J. Murphy and J. P. Riley, A modified single solution method for the determination of phosphate in natural waters, *Analytica Chimica Acta*, 1962, **27**, 31-36.
50. Stainton MP, Capel MJ and F. Armstrong, The chemical analysis of freshwater., *Bull. Fish. Res Board Can.*, 1974, 125.
51. M. Hupfer, D. Zak, R. Roβberg, C. Herzog and R. Pöthig, Evaluation of a well-established sequential phosphorus fractionation technique for use in calcite-rich lake sediments: identification and prevention of artifacts due to apatite formation, *Limnology and Oceanography: Methods*, 2009, **7**, 399-410.
52. B. J. Huser, Sequential fractionation of phosphorus in sediment, 2019, 20.
53. B. J. Cade-Menun, C. R. Benitez-Nelson, P. Pellechia and A. Paytan, Refining 31P nuclear magnetic resonance spectroscopy for marine particulate samples: Storage conditions and extraction recovery, *Marine Chemistry*, 2005, **97**, 293-306.
54. A. Pannard, B. E. Beisner, D. F. Bird, J. Braun, D. Planas and M. Bormans, Recurrent internal waves in a small lake: Potential ecological consequences for metalimnetic phytoplankton populations, *Limnology and Oceanography: Fluids and Environments*, 2011, **1**, 91-109.
55. D. Planas and S. Paquet, Importance of climate change-physical forcing on the increase of cyanobacterial blooms in a small, stratified lake, *Journal of Limnology*, 2016, **75**.
56. NICNAS, *Existing chemical secondary notification: Phoslock™*, Report NA/899S, 2014.
57. J. D. Cline, Spectrophotometric detemination of hydrogen sulfide in natural waters., *Limnology and Oceanography*, 1969, **14**, 454-458.
58. D. L. Parkhurst and C. A. J. Appelo, *Description of input and examples for PHREEQC version 3—A computer program for speciation, batch-reaction, one-dimensional transport, and inverse geochemical calculations: U.S. Geological Survey Techniques and Methods*, 2013.
59. E. Tipping, S. Lofts and J. E. Sonke, Humic Ion-Binding Model VII: a revised parameterisation of cation-binding by humic substances, *Environmental Chemistry*, 2011, **8**, 225-235.
60. S. Lofts, E. Tipping and J. Hamilton-Taylor, The Chemical speciation of Fe(III) in freshwaters, *Aquatic Geochemistry*, 2008, **14**, 337-358.

View Article Online
DOI: 10.1039/D1EM00544H

61. R. Marsac, C. Catrouillet, M. Davranche, M. Bouhnik-Le Coz, N. Briant, N. Janot, A. Otero-Fariña, J. E. Groenenberg, M. Pédrot and A. Dia, Modeling rare earth elements binding to humic acids with model VII, *Chemical Geology*, 2021, **567**, 120099.
62. R. Marsac, M, N. Banik, L, J. Lützenkirchen, L, C. Catrouillet, C. Marquardt, M and K. Johannesson, H, Modeling metal ion-humic substances complexation in highly saline conditions, *Applied Geochemistry*, 2017, **79**, 52-64.
63. R. Marsac, N. L. Banik, C. M. Marquardt and J. V. Kratz, Stabilization of polynuclear plutonium(IV) species by humic acid, *Geochim Cosmochim Ac*, 2014, **131**, 290-300.
64. D. G. Kinniburgh and D. M. Cooper, PhreePlot: Creating graphical output with PHREEQC., 2011.
65. R.-M. Couture, C. Gobeil and A. Tessier, Arsenic, iron and sulfur co-diagenesis in lake sediments, *Geochim Cosmochim Ac*, 2010, **74**, 1238-1255.
66. É. Leclerc, J. J. Venkiteswaran, I. Jasiak, J. Telford, M. Schultz, B. Wolfe, R. Hall and R. M. Couture, Quantifying arsenic post-depositional mobility in lake sediments impacted by gold ore roasting in sub-arctic Canada using inverse diagenetic modelling, *Environmental Pollution*, 2021, **288**, 117723.
67. B. P. Boudreau, *Diagenetic models and their implementation: Modelling transport and reactions in aquatic sedimnets*, Springer, 1997.
68. P. Berg, N. Risgaard-Petersen and S. Rysgaard, Interpretation of measured concentration profiles in sediment pore water, *Limnology and Oceanography*, 1998, **43**, 1500-1510.
69. R. Shinohara, A. Imai, N. Kawasaki, K. Komatsu, A. Kohzu, S. Miura, T. Sano, T. Satou, N. Tomioka and K. Shimotori, Changes in the composition of phosphorus (P) compound groups in sediment and P in sediment pore water in a shallow eutrophic lake: a 31P NMR study, *Limnology*, 2016, DOI: 10.1007/s10201-016-0497-4, 1-11.
70. D. Planas and P. Juneau, *Rapport technique: projet de restauration du lac Bromont*, Report PASSI 38760, 2019.
71. D. Copetti, K. Finsterle, L. Marziali, F. Stefani, G. Tartari, G. Douglas, K. Reitzel, B. M. Spears, I. J. Winfield, G. Crosa, P. D'Haese, S. Yasseri and M. Lürling, Eutrophication management in surface waters using lanthanum modified bentonite: A review, *Water Res.*, 2016, **97**, 162-174.
72. S. Egemose, K. Reitzel, F. Andersen and M. R. Flindt, Chemical Lake Restoration Products: Sediment Stability and Phosphorus Dynamics, *Environmental Science & Technology*, 2010, **44**, 985-991.
73. M. Lürling and E. J. Faassen, Controlling toxic cyanobacteria: Effects of dredging and phosphorus-binding clay on cyanobacteria and microcystins, *Water Res.*, 2012, **46**, 1447-1459.
74. M. Lürling and Y. Tolman, Effects of lanthanum and lanthanum-modified clay on growth, survival and reproduction of Daphnia magna, *Water Res.*, 2010, **44**, 309-319.
75. G. Waajen, F. van Oosterhout, G. Douglas and M. Lürling, Management of eutrophication in Lake De Kuil (The Netherlands) using combined flocculant – Lanthanum modified bentonite treatment, *Water Res.*, 2016, **97**, 83-95.
76. G. Waajen, F. van Oosterhout, G. Douglas and M. Lürling, Geo-engineering experiments in two urban ponds to control eutrophication, *Water Res.*, 2016, **97**, 69-82.
77. H. Yin, G. B. Douglas, Y. Cai, C. Liu and D. Copetti, Remediation of internal phosphorus loads with modified clays, influence of fluvial suspended particulate matter

View Article Online
DOI: 10.1039/D1EM00544H

and response of the benthic macroinvertebrate community, *Science of The Total Environment*, 2018, **610-611**, 101-110.

78. L. Dithmer, A. S. Lipton, K. Reitzel, T. E. Warner, D. Lundberg and U. G. Nielsen, Characterization of Phosphate Sequestration by a Lanthanum Modified Bentonite Clay: A Solid-State NMR, EXAFS, and PXRD Study, *Environmental Science & Technology*, 2015, **49**, 4559-4566.
79. K. Reitzel, J. Ahlgren, H. DeBrabandere, M. Waldeback, A. Gogoll, L. Tranvik and E. Rydin, Degradation rates of organic phosphorus in lake sediment, *Biogeochemistry*, 2007, **82**, 15-28.
80. J. Ahlgren, K. Reitzel, L. Tranvik, A. Gogoll and E. Rydin, Degradation of organic phosphorus compounds in anoxic Baltic Sea sediments: A 31P nuclear magnetic resonance study, *Limnology and Oceanography*, 2006, **51**, 2341-2348.
81. M. Kong, F. Liu, Y. Tao, P. Wang, C. Wang and Y. Zhang, First attempt for in situ capping with lanthanum modified bentonite (LMB) on the immobilization and transformation of organic phosphorus at the sediment-water interface, *Science of The Total Environment*, 2020, **741**, 140342.
82. D. Rickard, Kinetics of pyrite formation by the H2S oxidation of iron (II) monosulfide in aqueous solutions between 25 and 125°C: The rate equation, *Geochim Cosmochim Ac*, 1997, **61**, 115-134.
83. M. Rothe, T. Frederichs, M. Eder, A. Kleeberg and M. Hupfer, Evidence for vivianite formation and its contribution to long-term phosphorus retention in a recent lake sediment: a novel analytical approach, *Biogeosciences*, 2014, **11**, 5169-5180.
84. M. Rothe, A. Kleeberg, B. Grüneberg, K. Friese, M. Pérez-Mayo and M. Hupfer, Sedimentary sulphur : iron ratio indicates vivianite occurrence: A study from two contrasting freshwater systems, *PLOS ONE*, 2015, **10**, e0143737.
85. U. Schwertmann, Solubility and dissolution of iron oxides, *Plant and Soil*, 1991, **130**, 1-25.
86. M. Søndergaard, E. Jeppesen, T. L. Lauridsen, C. Skov, E. H. Van nes, R. Roijackers, E. Lammens and R. Portielje, Lake restoration: successes, failures and long-term effects, *Journal of Applied Ecology*, 2007, **44**, 1095-1105.
87. D. Schindler, F. Armstrong, S. Holmgren and G. Brunskill, Eutrophication of Lake 227, Experimental Lakes Area, Northwestern Ontario, by Addition of Phosphate and Nitrate, *Journal of the Fisheries Research Board of Canada*, 1971, **28**, 1763-1782.
88. A. Kleeberg, C. Herzog and M. Hupfer, Redox sensitivity of iron in phosphorus binding does not impede lake restoration, *Water Res.*, 2013, **47**, 1491-1502.
89. C. T. Parsons, F. Rezanezhad, D. W. O'Connell and P. Van Cappellen, Sediment phosphorus speciation and mobility under dynamic redox conditions, *Biogeosciences*, 2017, **14**, 3585-3602.
90. C. Hyacinthe and P. Van Cappellen, An authigenic iron phosphate phase in estuarine sediments: composition, formation and chemical reactivity, *Marine Chemistry*, 2004, **91**, 227-251.
91. X. Li, Z. Zhang, Q. Xie, R. Yang, T. Guan and D. Wu, Immobilization and Release Behavior of Phosphorus on Phoslock-Inactivated Sediment under Conditions Simulating the Photic Zone in Eutrophic Shallow Lakes, *Environmental Science & Technology*, 2019, **53**, 12449-12457.

View Article Online
DOI: 10.1039/D1EM00544H

92. M. A. Zeller and M. J. Alperin, The efficacy of Phoslock® in reducing internal phosphate loading varies with bottom water oxygenation, *Water Research X*, 2021, **11**, 100095.
93. K. H. Tan, *Humic matter in soil and the environment: Principles and controversies*, CRC press, Taylor and Francis group., 2 edn., 2014.
94. X. Feng, A. J. Simpson and M. J. Simpson, Chemical and mineralogical controls on humic acid sorption to clay mineral surfaces, *Organic Geochemistry*, 2005, **36**, 1553-1566.
95. Y. Audette, D. S. Smith, C. T. Parsons, W. Chen, F. Rezanezhad and P. Van Cappellen, Phosphorus binding to soil organic matter via ternary complexes with calcium, *Chemosphere*, 2020, **260**, 127624.
96. J. Antelo, F. Arce and S. Fiol, Arsenate and phosphate adsorption on ferrihydrite nanoparticles. Synergetic interaction with calcium ions, *Chemical Geology*, 2015, **410**, 53-62.
97. M. Mucci, G. Douglas and M. Lürling, Lanthanum modified bentonite behaviour and efficiency in adsorbing phosphate in saline waters, *Chemosphere*, 2020, **249**, 126131.
98. F. H. Firsching and J. Mohammadzadei, Solubility products of the rare-earth carbonates, *Journal of Chemical & Engineering Data*, 1986, **31**, 40-42.
99. J. H. Lee and R. H. Byrne, Examination of comparative rare Earth element complexation behaviour using linear free-engergy relationships, *Geochim. Cosmochim. Acta*, 1992, **56**.
100. G. D. Klungness and R. H. Byrne, Comparative hydrolysis behavior of the rare earths and yttrium: the influence of temperature and ionic strength, *Polyhedron*, 2000, **19**, 99-107.
101. Y.-R. Luo and R. H. Byrne, Carbonate complexation of yttrium and the rare earth elements in natural waters, *Geochim Cosmochim Ac*, 2004, **68**, 691-699.
102. F. J. Millero, Stability constants for the formation of rare earth-inorganic complexes as a function of ionic strength, *Geochim Cosmochim Ac*, 1992, **56**, 3123-3132.
103. Y. Luo and F. J. Millero, Effects of temperature and ionic strength on the stabilities of the first and second fluoride complexes of yttrium and the rare earth elements, *Geochim Cosmochim Ac*, 2004, **68**, 4301-4308.
104. K. Spahiu and J. Bruno, *A selected thermodynamic database for REE to be used in HLNW performance assessment exercises*, Report 0284-3757, Sweden, 1995.
105. P. L. Brown and C. Ekberg, *Hydrolysis of metal ions*, Wiley-VCH Verlag GmbH & Co. KGaA-Weinheim, 2016.
106. I. I. Diakonov, K. V. Ragnarsdottir and B. R. Tagirov, Standard thermodynamic properties and heat capacity equations of rare earth hydroxides:: II. Ce(III)-, Pr-, Sm-, Eu(III)-, Gd-, Tb-, Dy-, Ho-, Er-, Tm-, Yb-, and Y-hydroxides. Comparison of thermochemical and solubility data, *Chemical Geology*, 1998, **151**, 327-347.
107. X. Liu and R. H. Byrne, Rare earth and yttrium phosphate solubilities in aqueous solution, *Geochim Cosmochim Ac*, 1997, **61**, 1625-1633.

View Article Online
DOI: 10.1039/D1EM00544H

Fig. 1 Location and bathymetry of Lake Bromont, along with sampling site locations (circles) and lake outlet (triangle).

Fig. 2 Phosphorus partitioning determined by SEQ within the first 0-4 cm of the sediment surface at the Deep, House and Inflow sites before (white) and after (colour) the Phoslock™ treatment. BD, NaOH and HCl extractions are identified by light, medium and dark shades, respectively, as well as on the X-axis. Error bars indicate the outcome of triplicate SEQ.

Fig. 3 Vertical distribution of total P (shaded symbols), soluble reactive P (open symbols (panels a,e,i) and total La and Fe concentrations in the SEQ BD (cirlces), NaOH (triangle) and HCl (square) fractions, along with total organic C and C:N ratios in the sediment of the Deep (a-d), House (e-h) and Inflow (i-l) sites.

Fig. 4 Upper panel: Distribution of sedimentary P species identified by ^{31}P NMR at depths above, at and just below the sedimentary La concentration maximum at the Deep, House and Inflow sites. Lower panel: Solution ^{31}P NMR analysis of the NaOH-EDTA extracts at depths selected, above, at or just below sedimentary La concentration maximum (see Fig. 3) at the Deep, House and Inflow sites.

Fig. 5 Porewater concentration profiles of P (circles), La (squares), Fe (triangles), SO_4^{2-} (solid inverted triangles), ΣS^{-II} (open inverted triangle) and DOC (diamonds) at the Deep (a-e), House (f-j), and Inflow (k-o) sites. The horizontal dashed line indicates the sediment-water interface. ΣS^{-II} were below detection limit of 0.7 μmol L^{-1} at the Deep site.

Fig. 6 Measured DOC:P and DOC:La ratios as a function of depth at the Deep, House and Inflow sites along with model-predicted saturation index (SI) of the porewater with respect to $LaPO_{4(s)}$

View Article Online
DOI: 10.1039/D1EM00544H

with (solid line) and without (dashed line) accounting for the effect of DOC on aqueous La speciation (panel a,f,i).

Fig. 7 Model-predicted speciation (%) of La as function of both dissolved Fe^{2+} and DOC under geochemical conditions prevailing at lake Bromont**.** The upper left zone represents a system where $LaPO_{4(s)}$ dominates, while the lower right zone represents a system where DOC binds La^{3+} and hinders $LaPO_{4(s)}$ formation.

View Article Online
DOI: 10.1039/D1EM00544H

Table 1. Summary of the phosphorus sequential extraction scheme.

Step	Extractant	Duration (hrs)	Target P phase
1	Oxygen-free H_2O	2	Loosely bound P
2	0.11 M Bicarbonate/Dithionite, pH 7	1	Bound to redox sensitive Fe and/or Mn oxides and P_{org}
3	0.1 M NaOH	16	Bound to Fe/Al oxides and comprising microorganisms, detritus and humic substances (P_{org})
4	0.5 M HCl	16	Bound to apatite and La

Table 2. Reactions for the formation of the various La species and their corresponding equilibrium constants added to PHREEQC.

Reaction	Log K_{eq}	Ref.
$Ln^{3+} + H_2O \rightleftharpoons LnOH^{2+} + H^+$	-8.81	99, 100
$Ln^{3+} + 2\ H_2O \rightleftharpoons Ln(OH)_2^+ + 2H^+$	-18.14	99, 100
$Ln^{3+} + 3\ H_2O \rightleftharpoons Ln(OH)_{3(aq)} + 3H^+$	-27.90	99, 100
$Ln^{3+} + HCO_3^- \rightleftharpoons LnHCO_3^{2+}$	2.34	101
$Ln^{3+} + CO_3^{2-} \rightleftharpoons LnCO_3^+$	6.73	101
$Ln^{3+} + 2\ CO_3^{2-} \rightleftharpoons Ln(CO_3)_2^-$	11.3	101
$Ln^{3+} + Cl^- \rightleftharpoons LnCl^{2+}$	0.65	101
$Ln^{3+} + NO_3^- \rightleftharpoons LnNO_3^{2+}$	0.58	102
$Ln^{3+} + F^- \rightleftharpoons LnF^{2+}$	3.11	103
$Ln^{3+} + H_2PO_4^- \rightleftharpoons LnH_2PO_4^{2+}$	2.5	104
$Ln^{3+} + HPO_4^{2-} \rightleftharpoons LnHPO_4^+$	5.1	104
$Ln^{3+} + 2\ HPO_4^{2-} \rightleftharpoons Ln(HPO_4)_2^-$	8.4	104
$Ln^{3+} + PO_4^{3-} \rightleftharpoons LnPO_{4(aq)}$	10.96	104
$Ln^{3+} + 2\ PO_4^{3-} \rightleftharpoons Ln(PO_4)_2^{-3}$	17.6	104
$Ln^{3+} + SO_4^{2-} \rightleftharpoons LnSO_4^+$	3.4	104
$Ln^{3+} + 2\ SO_4^{2-} \rightleftharpoons Ln(SO_4)_2^-$	5.1	104
$Ln_2(CO_3)_{3(s)} \rightleftharpoons 2Ln^{3+}_{(aq)} + 3CO_3^{2-}{}_{(aq)}$	-29.91	98
$Ln(OH)_{3(s)} + 3H^+ \rightleftharpoons Ln^{3+} + 3H_2O$	19.72	105
$Ln(OH)_{3(am,fresh)} + 3H^+ \rightleftharpoons Ln^{3+} + 3H_2O$	21.94	106
$LnPO_{4(s)} \rightleftharpoons Ln^{3+} + PO_4^{3-}$	-25.75	107

View Article Online
DOI: 10.1039/D1EM00544H

Table 3. Fluxes of P, La and Fe across the sediment-water interface (SWI) calculated via inverse diagenetic modelling using PROFILE. Positive values indicate transport from the sediment to the water column. Units of mass are used instead of molar units for comparisons with previous estimates and other sites.

	Flux across the SWI (mg m^{-2} d^{-1})		
	La	**P**	**Fe**
Deep site	$+2.1 \times 10^{-7}$	+ 2.5	+40
House site	$+1.1 \times 10^{-7}$	- 0.2	+7.2
Inflow site	$+1.3 \times 10^{-7}$	+ 1.0	+8.3

View Article Online
DOI: 10.1039/D1EM00544H

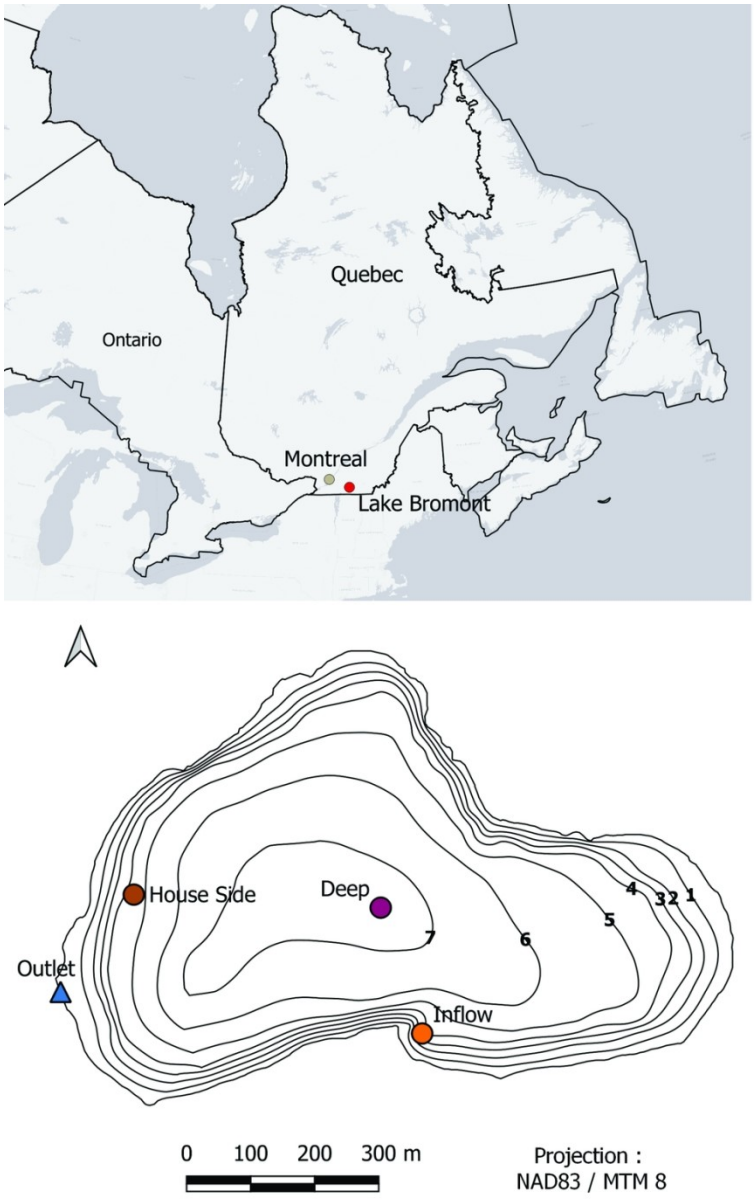

Fig. 1 Location and bathymetry of Lake Bromont, along with sampling site locations (circles) and lake outlet (triangle).

83x133mm (300 x 300 DPI)

View Article Online
DOI: 10.1039/D1EM00544H

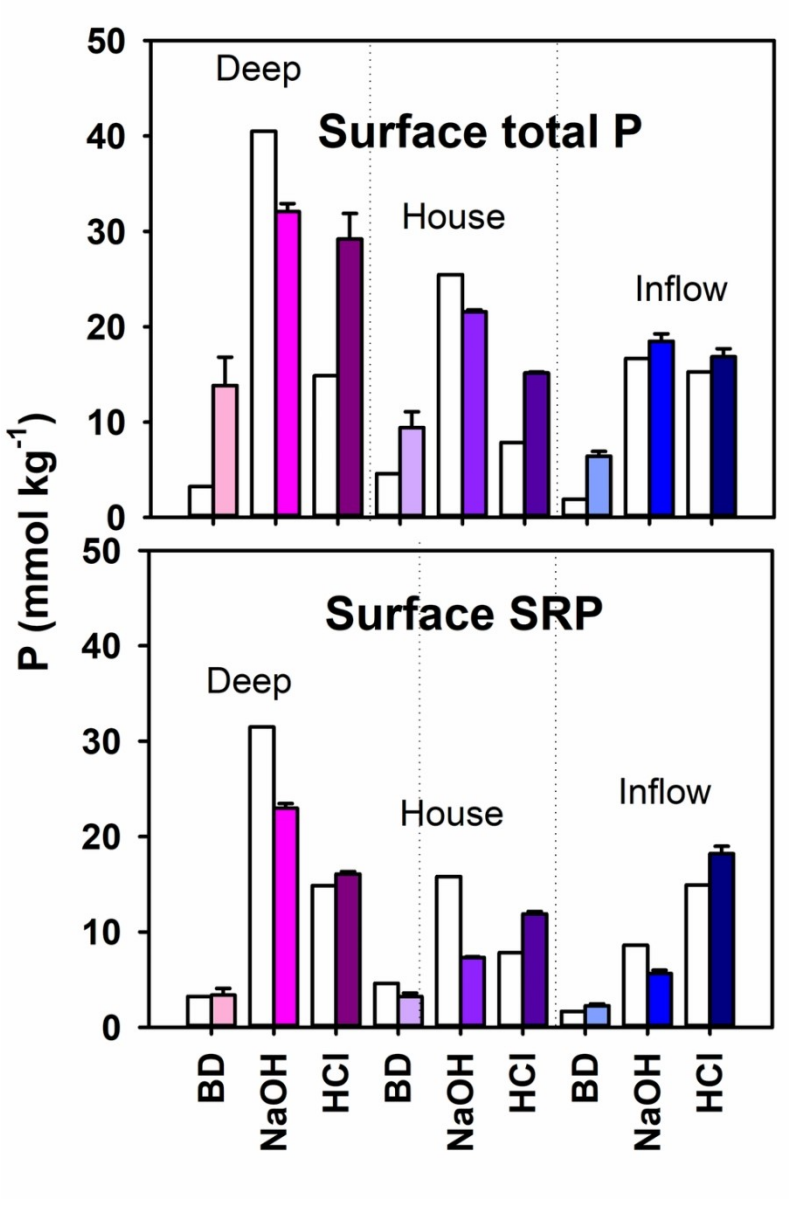

Fig. 2 Phosphorus partitioning determined by SEQ within the first 0-4 cm of the sediment surface at the Deep, House and Inflow sites before (white) and after (colour) the PhoslockTM treatment. BD, NaOH and HCl extractions are identified by light, medium and dark shades, respectively, as well as on the X-axis.

82x126mm (300 x 300 DPI)

View Article Online
DOI: 10.1039/D1EM00544H

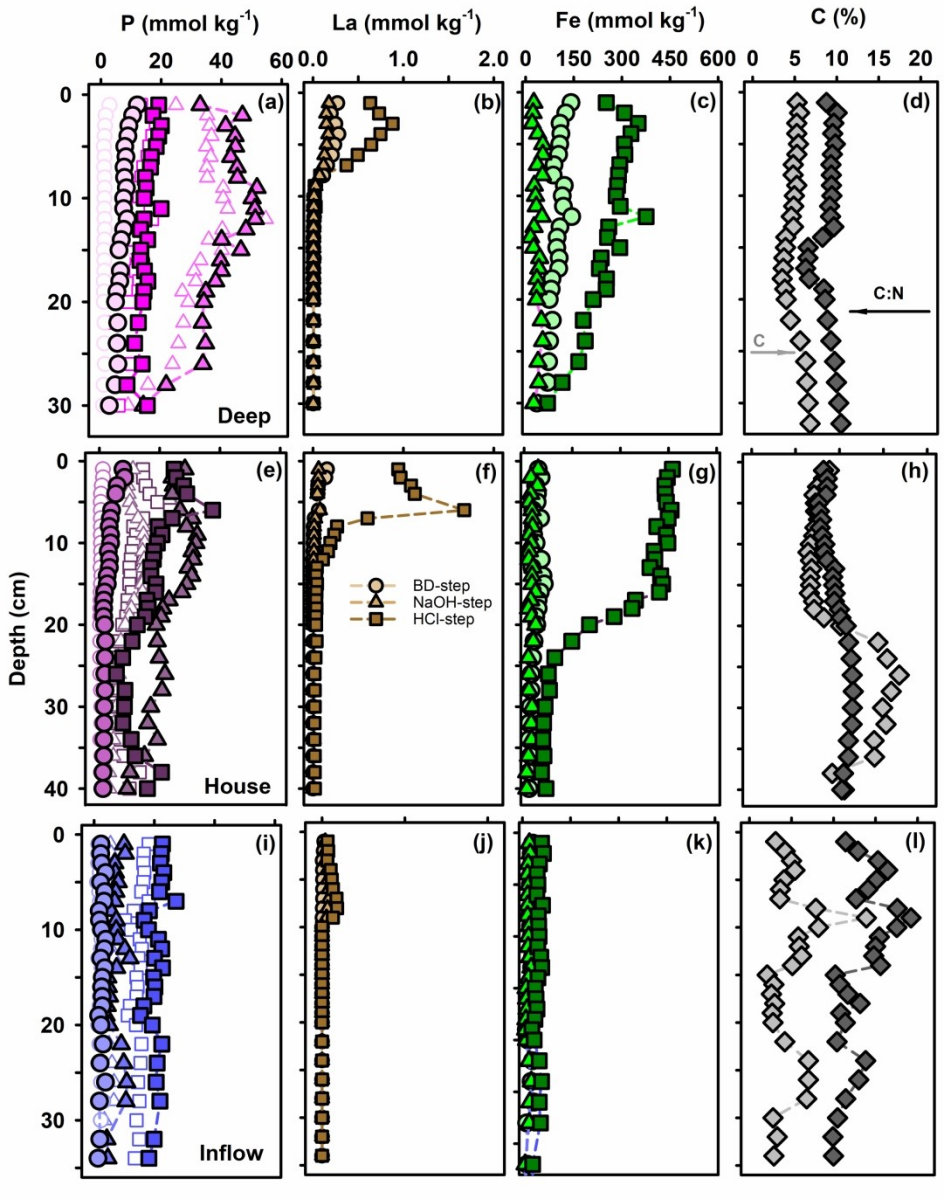

Fig. 3 Vertical distribution of total P (shaded symbols), soluble reactive P (open symbols (panels a,e,i) and total La and Fe concentrations in the SEQ BD (cirlces), NaOH (triangle) and HCl (square) fractions, along with total organic C and C:N ratios in the sediment of the Deep (a-d), House (e-h) and Inflow (i-l) sites.

233x295mm (300 x 300 DPI)

View Article Online
DOI: 10.1039/D1EM00544H

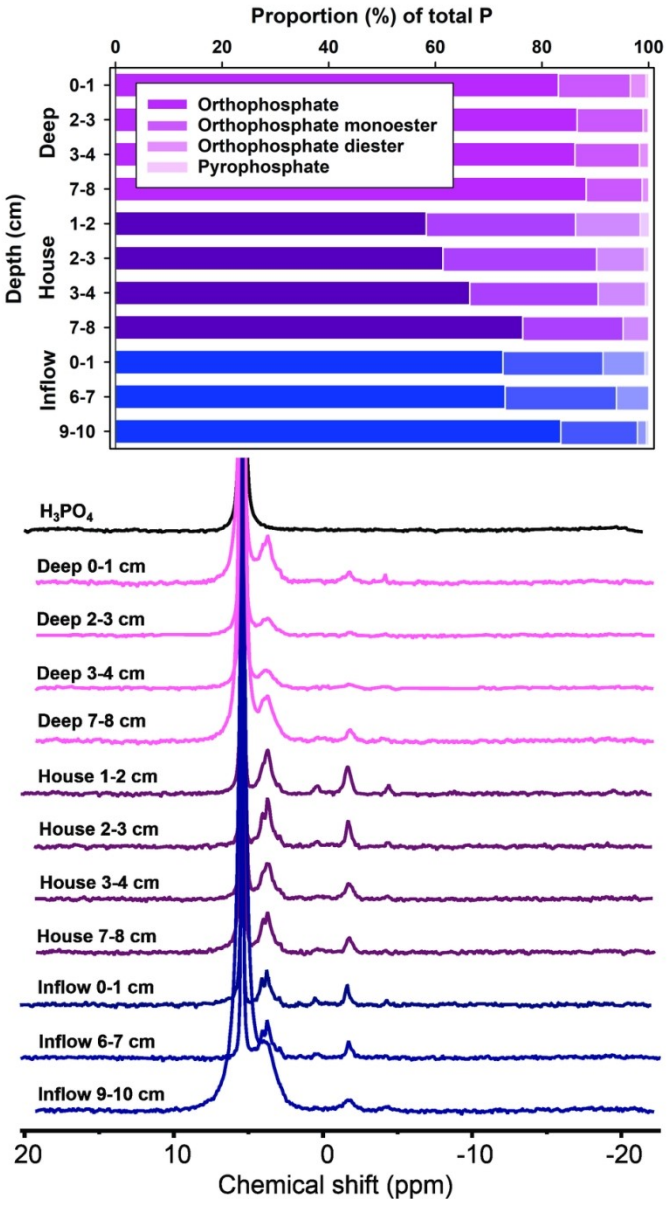

Fig. 4 Upper panel: Distribution of sedimentary P species identified by ^{31}P NMR at depths above, at and just below the sedimentary La concentration maximum at the Deep, House and Inflow sites. Lower panel: Solution ^{31}P NMR analysis of the NaOH-EDTA extracts at depths selected, above, at or just below sedimentary La concentration maximum (see Fig. 3) at the Deep, House and Inflow sites.

82x143mm (300 x 300 DPI)

View Article Online
DOI: 10.1039/D1EM00544H

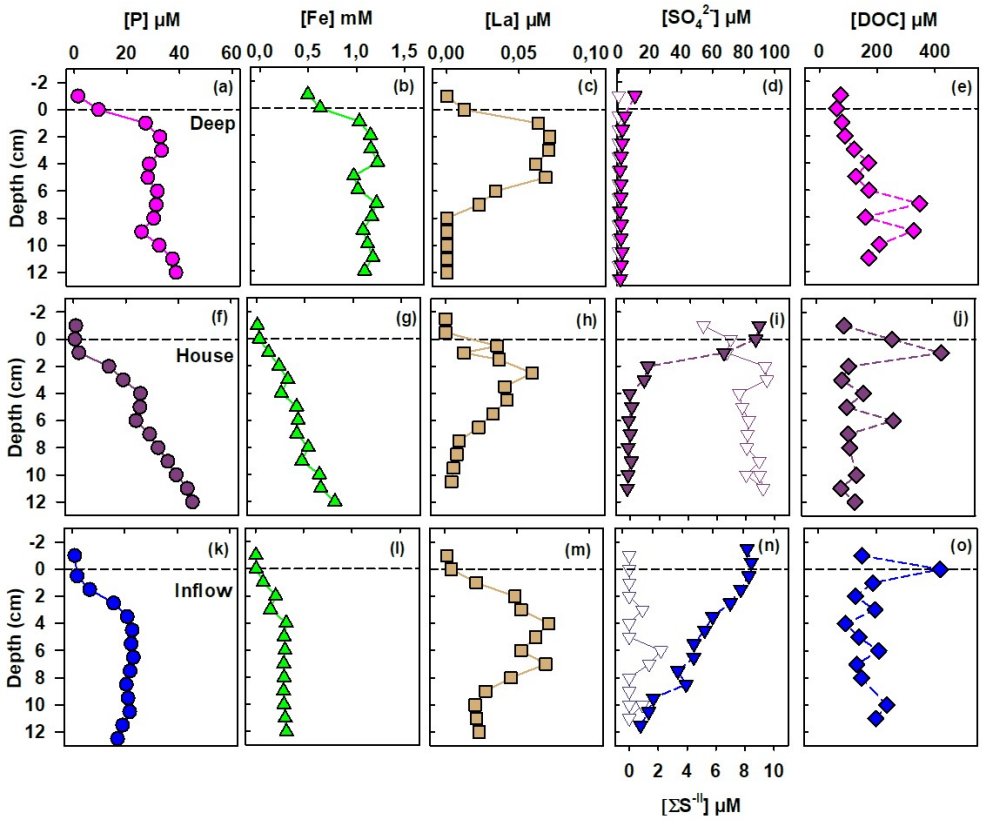

Fig. 5 Porewater concentration profiles of P (circles), La (squares), Fe (triangles), SO_4^{2-} (solid inverted triangles), ΣS^{-II} (open inverted triangle) and DOC (diamonds) at the Deep (a-e), House (f-j), and Inflow (k-o) sites. The horizontal dashed line indicates the sediment-water interface. ΣS^{-II} were below detection limit of 0.7 µmol L^{-1} at the Deep site.

291x240mm (100 x 100 DPI)

View Article Online
DOI: 10.1039/D1EM00544H

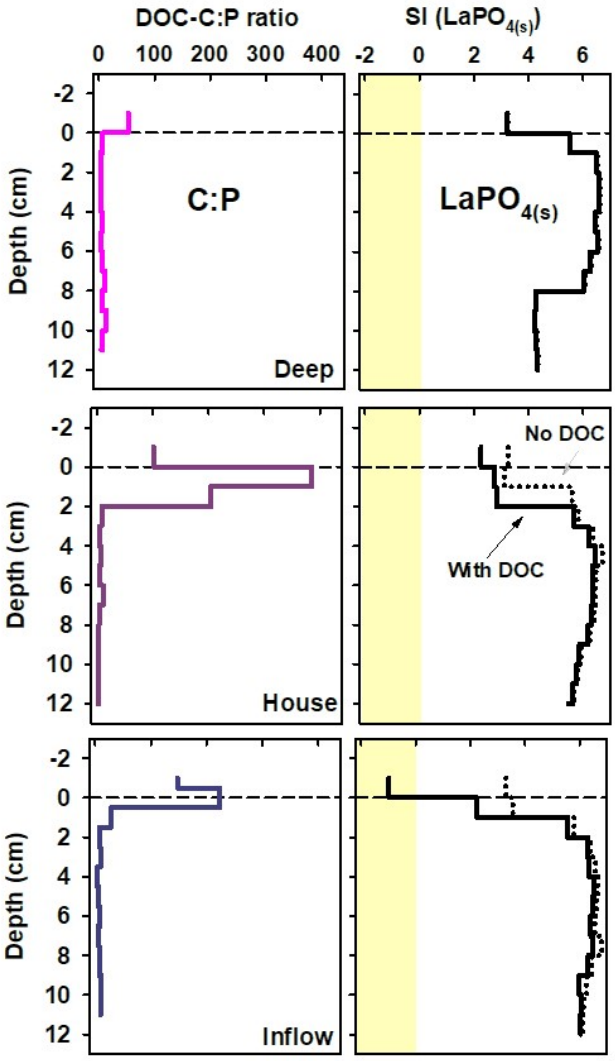

Fig. 6 Measured DOC:P and DOC:La ratios as a function of depth at the Deep, House and Inflow sites along with model-predicted saturation index (SI) of the porewater with respect to $LaPO_{4(s)}$ with (solid line) and without (dashed line) accounting for the effect of DOC on aqueous La speciation (panel a,f,i).

151x241mm (100 x 100 DPI)

View Article Online
DOI: 10.1039/D1EM00544H

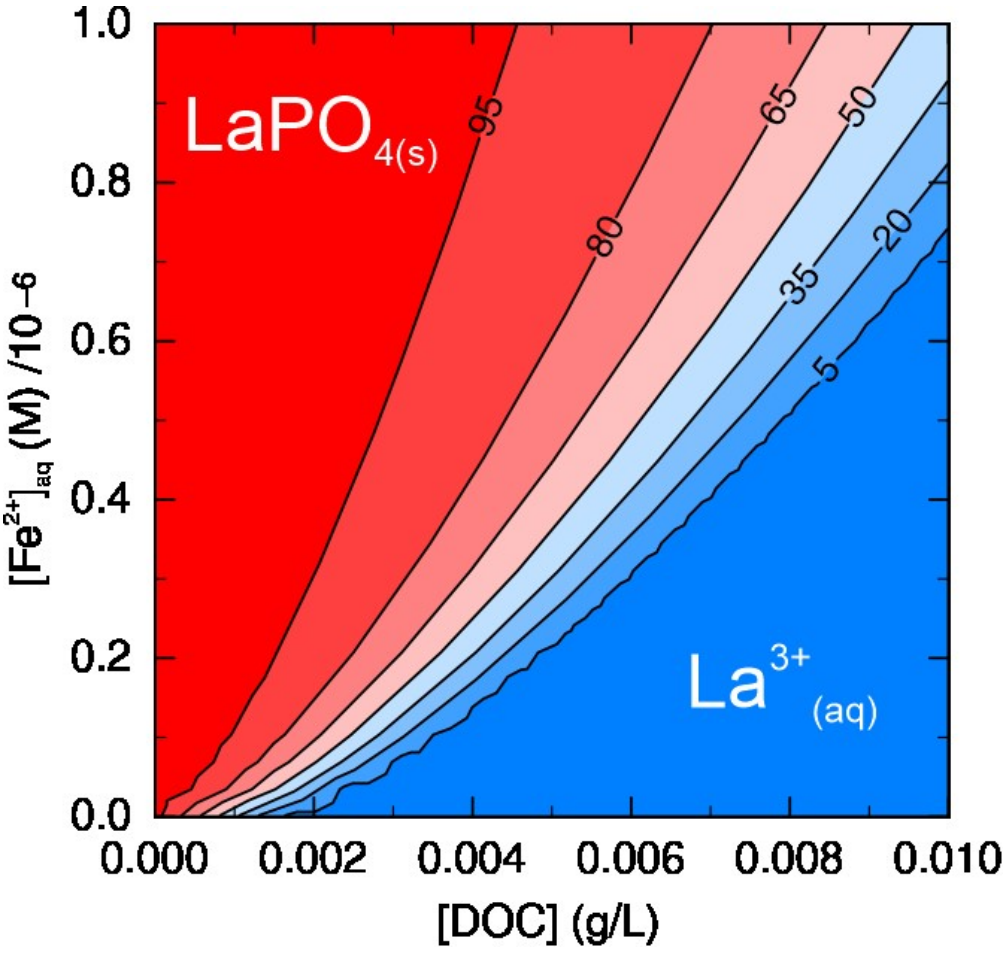

Fig. 7 Model-predicted speciation (%) of La as function of both dissolved Fe^{2+} and DOC under geochemical conditions prevailing at lake Bromont. The upper left zone represents a system where $LaPO_{4(s)}$ dominates, while the lower right zone represents a system where DOC binds La^{3+} and hinders $LaPO_{4(s)}$ formation.